

Battery Discharge Modeling for Electric Vehicles: A Hybrid Physics-based Residual Learning Approach

Praharshitha Aryasomayajula¹, Ting Bai², and Andreas A. Malikopoulos², *Senior Member, IEEE*

Abstract—The growing integration of electric vehicle (EV) fleets into transportation services and energy systems requires accurate modeling of battery discharge and state-of-charge (SoC) evolution to ensure reliable vehicle operation and grid coordination. Existing approaches face a trade-off between interpretable but simplified physics-based models and data-driven methods that demand large datasets and may lack physical consistency. In this paper, we propose a hybrid physics-based residual learning framework for EV battery discharge modeling. A vehicle dynamics model based on force-balance equations provides an interpretable baseline estimate of energy consumption and SoC evolution, capturing aerodynamic drag, rolling resistance, and regenerative braking. A neural network residual learner then corrects discrepancies caused by complex factors such as traffic conditions and driver behavior. Experimental results on 1,500 trip scenarios demonstrate that the proposed approach reduces the mean absolute percentage error to approximately 0.8%, significantly outperforming physics-only models while preserving physical interpretability and computational efficiency.

I. INTRODUCTION

The rapid electrification of transportation systems is fundamentally reshaping urban mobility, with global electric vehicle (EV) sales exceeding 14 million units in 2023 and projected to reach 40 million by 2030 [1]. Unlike conventional vehicles that only consume energy, EVs can operate as mobile energy storage units capable of bidirectional interaction with the power grid [2], [3]. For instance, commercial fleets may charge their batteries during off-peak hours and discharge energy back to the grid during demand peaks, to support grid stability while reducing operational costs. Realizing such capabilities, however, requires accurate prediction of battery state-of-charge (SoC) evolution throughout vehicle trips. This entails forecasting energy consumption under varying routes, driving behaviors, and traffic conditions. Reliable SoC estimation is thus essential not only for improving EV trip planning [4], [5] and battery management but also for enabling grid operators to anticipate aggregated charging demand [6] when large fleets rely on the shared charging infrastructure.

Accurate battery discharge prediction is also fundamental for system-level coordination in emerging electric mobility

ecosystems. In autonomous mobility-on-demand systems, joint routing, rebalancing, and charging scheduling decisions critically depend on reliable energy consumption models [7]. Moreover, connectivity-enabled coordination among vehicles can substantially affect energy consumption patterns and battery degradation dynamics [8]. At the vehicle level, control-oriented frameworks for hybrid and electrified powertrains have demonstrated how energy management strategies influence performance, efficiency, and battery usage [9], [10].

Existing EV energy consumption modeling approaches fall into three categories, each with distinct limitations. Physics-based models [11]–[13] estimate energy consumption from vehicle dynamics and powertrain characteristics. While physically interpretable, these models are often built upon simplified assumptions, such as flat terrain, constant velocity, and idealized driving cycles, and fail to capture real-world factors including elevation variations, stop-and-go traffic, and driver-specific behavior. As a result, their prediction accuracy remains around 5–8% [14], whereas real-world energy consumption can vary by as much as 40–80% depending on operating conditions [15]. Data-driven models [16], [17] instead learn consumption patterns directly from historical driving data and can reduce prediction errors to approximately 2–3%. However, these approaches typically require large volumes of training data, offer limited interpretability, and may struggle to generalize to unseen operating conditions. Black-box prediction models [18], [19], based on complex machine learning architectures, further improve predictive accuracy but sacrifice interpretability and physical consistency. The opaque decision mechanisms could result in unreliable predictions outside the training distribution, undermining driver trust and exacerbating range anxiety [20], [21]. Moreover, the lack of physical constraints makes it difficult for grid operators to verify whether predicted energy consumption keeps consistent with fundamental energy conservation principles.

Recent hybrid approaches attempt to combine the strengths of physics-based and data-driven methods. For example, Morlock et al. [22] integrated simplified physical models with Gaussian processes, while Liu et al. [23] proposed physics-guided neural networks to incorporate prior physical knowledge into learning-based frameworks. Despite these advances, existing hybrid methods exhibit several notable limitations. Some rely on simplified physical models that fail to capture the complexity of real-world driving conditions. Others require sophisticated constraint formulations involving Lagrangian multipliers or customized optimization

*This research was supported in part by NSF under Grants CNS-2401007, CMMI-234881, IIS-2415478, and in part by MathWorks.

Praharshitha Aryasomayajula is with the School of Mechanical and Aerospace Engineering, Cornell University, Ithaca, New York, USA. E-mail: la459@cornell.edu

T. Bai, and A. A. Malikopoulos are with the School of Civil & Environmental Engineering, Cornell University, Ithaca, New York, USA. E-mails: {tingbai, amaliko}@cornell.edu

procedures, which limit their practical deployment [24]. To date, no approach achieves a good balance among high prediction accuracy, physical interpretability, computational efficiency, and low data requirements.

This paper focuses on accurate range prediction for EV drivers, where the proposed battery discharge modeling approach also provides a foundation for future grid integration applications. We develop a hybrid physics-informed machine learning framework based on residual learning [25], [26]. Our key innovation is to train a neural network to learn only the residual corrections to physics-based predictions, rather than simplifying the underlying physics or imposing complex training constraints. The physics component computes baseline energy consumption using detailed vehicle dynamics, while the neural network captures additional effects arising from terrain, traffic conditions, and driver behavior. This design preserves physical interpretability, requires limited training data, and maintains computational efficiency. The main contributions of this paper are as follows: (i) We present a comprehensive physics-based battery discharge model that incorporates three empirically derived driving profiles and realistic regenerative braking, providing reliable baseline energy predictions. (ii) We further develop a hybrid residual learning architecture that integrates detailed physics-based vehicle dynamics with neural network error correction. The architecture achieves high prediction accuracy without requiring complex constraint optimization. Experimental validation using realistic data demonstrates that the proposed modeling approach achieves a 62% reduction in prediction error while maintaining computational efficiency. Our results also reveal that driving behavior can cause up to 79% variation in energy consumption, providing important insights for EV range estimation.

The rest of this paper is organized as follows. In section II, we present the physics-based discharge model. In Section III, we introduce the machine learning residual model. In Section IV, we integrate these components into the proposed hybrid architecture, and then, in Section V, we present the experimental validation and performance evaluation. Finally, in Section VI, we discuss the key findings.

II. PHYSICS-BASED DISCHARGE MODEL

This section presents the physics-based battery discharge model. We first introduce the problem formulation and driving behavior profiles. Next, the vehicle power consumption model and its computational implementation are described, followed by model validation with realistic driving data.

A. Problem Formulation

A battery discharge session characterizes the energy consumption of an EV as it travels from an initial SoC to a final SoC. We represent a discharge session by the tuple

$$\mathcal{D} = (s_0, s_f, d, \bar{v}, \alpha), \quad (1)$$

where $s_0 \in [0, 1]$ denotes the initial SoC and $s_f \in [0, 1]$ is the final SoC with $s_f < s_0$. The variables $d \in \mathbb{R}^+$ and $\bar{v} \in \mathbb{R}^+$ represents the trip distance (km) and average velocity (km/h),

TABLE I
PARAMETERS OF THREE TYPICAL DRIVING PROFILES.

Parameter	Eco	Normal	Aggressive
Max Accel. (m/s ²)	1.5	2.5	4.0
Efficiency Multiplier	0.85	1.00	1.35
Regen Efficiency	0.75	0.65	0.50
Aux Power (kW)	0.0	0.5	1.5
Accel Phase (%)	20	30	40
Cruise Phase (%)	65	50	35
Brake Phase (%)	15	20	25

respectively, where \mathbb{R}^+ denotes the set of positive real numbers. Moreover, $\alpha \in \{\text{eco, normal, aggressive}\}$ denotes the driving behavior profile.

The total energy consumed during a trip is denoted as

$$E = C(s_0 - s_f),$$

where C denotes the battery capacity (kWh). In practice, however, the discharge power varies nonlinearly with vehicle velocity, acceleration, driving behavior, and environmental conditions. Consequently, the total energy consumption can be expressed as the time integral of the instantaneous power along the trip trajectory

$$E = \int_0^T P(t, v(t), a(t), s(t), \alpha) dt, \quad (2)$$

where P is the instantaneous discharge power (kW), T is the total trip duration (s), $v(t)$ and $a(t)$ denote the instantaneous velocity (m/s) and acceleration (m/s²), respectively, and $s(t)$ denotes the SoC at time t .

Based on the above formulation, the problem addressed in this paper is defined as follows: given the initial SoC s_0 , vehicle parameters, trip characteristics, and driving behavior, predict the final SoC s_f after completing the trip.

B. Driving Behavior Profiles

We model three distinct driving behaviors that significantly affect energy consumption, as summarized in Table I.

1) *Eco driving*: Eco driving emphasizes energy efficiency through gentle acceleration, anticipatory braking with maximum regeneration, and minimal auxiliary power usage. The corresponding efficiency parameters are defined as

$$\eta_e = 0.85, \quad \eta_e^r = 0.75, \quad (3)$$

where η_e denotes the eco driving efficiency multiplier and η_e^r represents the regenerative braking efficiency.

2) *Normal driving*: This driving behavior represents typical urban and highway commuting with moderate acceleration, standard regenerative braking, and typical auxiliary loads. Accordingly, the efficiency parameters are given by

$$\eta_n = 1.0, \quad \eta_n^r = 0.65, \quad (4)$$

where η_n denotes the efficiency multiplier for normal driving (baseline), and η_n^r is the regenerative braking efficiency.

3) *Aggressive driving*: Aggressive driving maximizes performance through hard acceleration, frequent rapid speed changes, and maximum auxiliary power. The corresponding efficiency parameters are depicted as

$$\eta_a = 1.35, \quad \eta_a^r = 0.50, \quad (5)$$

where η_a denotes the efficiency multiplier for aggressive driving and η_a^r is the regenerative braking efficiency.

C. Power Consumption Model

The total battery discharge power during a trip consists of three components: traction power $P_t(t)$ for vehicle motion, auxiliary system power $P_a(t)$, and power recovered through regenerative braking $P_r(t)$. Accordingly, the discharge power is denoted as

$$P(t) = P_t(t) + P_a(t) - P_r(t). \quad (6)$$

The traction power requirement derives from fundamental vehicle dynamics through force balance equations. We account for four primary resistance forces that oppose vehicle motion: rolling resistance from tire-road contact, aerodynamic drag from air resistance, grade resistance from road incline, and inertial force from acceleration. The instantaneous traction power is captured by

$$P_t(t) = \frac{1}{\eta_d} (F_r + F_a(t) + F_g + F_i(t)) \cdot v(t), \quad (7)$$

where $v(t)$ and $a(t)$ denote the instantaneous velocity (m/s) and acceleration (m/s²) at time t , respectively, and η_d is the drivetrain efficiency accounting for motor, inverter, and transmission losses. The individual force components are given by

$$F_r = C_r \cdot m \cdot g \cdot \cos(\theta), \quad (8)$$

$$F_a(t) = \frac{1}{2} \rho \cdot C_d \cdot A \cdot v(t)^2, \quad (9)$$

$$F_g = m \cdot g \cdot \sin(\theta), \quad (10)$$

$$F_i(t) = m \cdot a(t), \quad (11)$$

where θ represents the road grade angle (rad), with other involved parameters being provided in Table II.

The auxiliary system power $P_a(t)$ depends on driving behavior and environmental conditions, and is modeled as

$$P_a(t) = P_b + P_c(T) + P_m(\alpha, t), \quad (12)$$

where $P_b = 0.5$ kW is the base auxiliary power, $P_c(T)$ denotes the climate-dependent power, and $P_m(\alpha)$ is the mode-specific power at time t , with α indicating the driving mode profile. Based on typical HVAC system requirements [27], $P_c(T)$ is captured as

$$P_c(T) = \begin{cases} 2.0 \text{ kW}, & \text{if } T < 0^\circ\text{C}, \\ 1.0 \text{ kW}, & \text{if } 0^\circ\text{C} \leq T < 15^\circ\text{C}, \\ 0.5 \text{ kW}, & \text{if } 15^\circ\text{C} \leq T \leq 25^\circ\text{C}, \\ 2.5 \text{ kW}, & \text{otherwise,} \end{cases} \quad (13)$$

TABLE II
VEHICLE AND ENVIRONMENTAL PARAMETERS.

Parameter	Notation	Value
Battery Capacity (kWh)	C	75
Vehicle Mass (kg)	m	1800
Drag Coefficient	C_d	0.24
Frontal Area (m ²)	A	2.3
Rolling Resistance Coefficient	C_r	0.01
Drivetrain Efficiency	η_d	0.90
Air Density (kg/m ³)	ρ	1.225
Gravitational Acceleration (m/s ²)	g	9.81

where T denotes the ambient temperature. Accordingly, the driving mode-specific power is modeled as

$$P_m(\alpha, t) = \begin{cases} 0.0 \text{ kW}, & \text{if } \alpha = \text{eco at time } t, \\ 0.5 \text{ kW}, & \text{if } \alpha = \text{normal at time } t, \\ 1.5 \text{ kW}, & \text{if } \alpha = \text{aggressive at time } t. \end{cases} \quad (14)$$

During deceleration, regenerative braking recovers energy according to

$$P_r(t) = \begin{cases} \eta^r \cdot F_b \cdot v(t), & \text{if } a(t) < 0, \\ 0, & \text{otherwise,} \end{cases} \quad (15)$$

where the braking force is

$$F_b = m \cdot |a(t)|,$$

and η^r is determined by the driving mode as specified in Section II.B.

D. Computational Implementation

For practical computation, we discretize the trip into N time segments. The corresponding time step is given by

$$\Delta t = \frac{d \cdot 1000}{\bar{v} \cdot 3.6 \cdot N}, \quad (16)$$

where, as defined in (1), d is the trip distance (km) and \bar{v} is the average velocity (km/h). Here, Δt is measured in seconds. At each time step $t_k = k\Delta t$, a driving phase is assigned according to the profile-specific phase distribution in Table I. Let $\Delta v(t_k, \alpha)$ denote a stochastic velocity perturbation sampled from a normal distribution with standard deviation proportional to the driving aggressiveness. Then, the velocity at time step t_k follows

$$v(t_k) = \bar{v} + \Delta v(t_k, \alpha). \quad (17)$$

The acceleration in mode α at time t_k is denoted as

$$a(t_k, \alpha) = \begin{cases} 0.7a_{\max}(\alpha), & \text{if in acceleration phase at } t_k, \\ 0, & \text{if in cruise phase at } t_k, \\ -0.7a_{\max}(\alpha), & \text{if in braking phase at } t_k, \end{cases}$$

where $a_{\max}(\alpha)$ denotes the maximum acceleration under driving mode α . Given the above, the energy consumed at each time step is expressed as

$$\Delta E_k = P(t_k) \cdot \Delta t.$$

TABLE III

PHYSICS MODEL VALIDATION AGAINST LITERATURE BENCHMARKS.

Source	Velocity (km/h)	Reported (kWh/km)	Our Model (kWh/km)	Error (%)
Fiori et al. [12]	50	0.180	0.185	2.8
EPA Range Test	90	0.200	0.198	1.0
De Cauwer et al. [14]	110	0.230	0.224	2.6
Yuan et al. [16]	100	0.265	0.268	1.1

Thus, the total energy consumption (kWh) during the entire trip is given by

$$E = \frac{1}{3600} \sum_{k=0}^{N-1} P(t_k) \cdot \Delta t.$$

Recall that C denotes the battery capacity. Accordingly, the final SoC is denoted as

$$s_f = \max\left(0, s_0 - \frac{E}{C}\right), \quad (18)$$

and the SoC trajectory over the trip is obtained as

$$s(t_k) = s_0 - \frac{1}{C} \sum_{i=0}^{k-1} \Delta E_i. \quad (19)$$

Remark 1: The proposed physics-based model provides a transparent and computationally efficient framework for estimating EV energy consumption. By explicitly modeling the four primary resistance forces, rolling resistance, aerodynamic drag, grade resistance, and inertial force, and incorporating driving-mode-specific efficiency parameters and regenerative braking, the model captures the key mechanisms governing battery discharge. This physical grounding ensures reliable baseline predictions in diverse operating conditions while maintaining full interpretability of each modeled component.

E. Physics-based Model Validation

To validate the proposed physics-based model against real-world energy consumption patterns, we compare its predictions with published data from peer-reviewed literature and manufacturer specifications. As shown in Table III, the comparison covers a range of representative studies at different speeds. The results demonstrate that our model achieves a mean absolute percentage error of 2.1% across diverse driving conditions. This validation demonstrates that our first-principles approach accurately captures fundamental energy consumption patterns, providing a strong foundation for hybrid enhancement.

III. LEARNING-BASED RESIDUAL CORRECTION MODEL

A. Motivation and Approach

While the physics-based model achieves smaller error against published benchmarks, it suffers from systematic biases due to simplified assumptions, including flat terrain, constant vehicle mass, idealized driving cycles, etc. Real-world factors not captured include terrain-induced elevation changes, traffic dynamics causing stop-and-go patterns,

driver variability within behavioral categories (studies show up to $\pm 15\%$ efficiency variation [15]), battery SoC effects on internal resistance, environmental conditions beyond temperature, such as wind and precipitation, and auxiliary usage patterns that deviate from our heuristics.

Modeling each factor explicitly would require extensive additional parameters such as route elevation profiles, real-time traffic data, individual driver history, and detailed battery state models. Many of these are difficult to obtain in practice and would increase computational complexity substantially. Instead, we employ a machine learning (ML)-based residual learning approach to correct the aggregate effects of these unmodeled factors. This approach, successful in fluid dynamics [26] and climate modeling [28], preserves physical consistency while improving accuracy through data-driven refinement.

We decompose the true energy consumption as

$$E^* = E_p + \Delta E, \quad (20)$$

where E^* is the actual measured energy consumption, E_p is the physics baseline prediction, and ΔE represents aggregate error from unmodeled factors. The residual learning objective trains a neural network f such that

$$\Delta E \approx f(\mathcal{X}, E_p; \theta), \quad (21)$$

where \mathcal{X} represents trip features and θ are learned neural network parameters.

B. Neural Network Architecture

We employ a feedforward neural network with 10 input features characterizing the trip: distance d , average velocity \bar{v} , maximum velocity v_{\max} , one-hot encoding of driving behavior α (3 features), ambient temperature T , time of day, initial SoC s_0 , physics prediction E_p , and consumption rate E_p/d . Including E_p as an input allows the network to learn multiplicative or additive corrections appropriate for different consumption regimes, while the consumption rate helps recognize scenarios where physics assumptions are particularly violated.

The architecture consists of three hidden layers with progressively decreasing dimensions and dropout regularization to mitigate overfitting. The hidden-layer activations are defined as

$$\mathbf{h}_1 = \text{ReLU}(\mathbf{W}_1 \mathbf{x} + \mathbf{b}_1) \in \mathbb{R}^{64}, \quad (22)$$

$$\mathbf{h}_2 = \text{Dropout}(\text{ReLU}(\mathbf{W}_2 \mathbf{h}_1 + \mathbf{b}_2), p = 0.2) \in \mathbb{R}^{32}, \quad (23)$$

$$\mathbf{h}_3 = \text{Dropout}(\text{ReLU}(\mathbf{W}_3 \mathbf{h}_2 + \mathbf{b}_3), p = 0.2) \in \mathbb{R}^{16}, \quad (24)$$

where \mathbf{W}_i and \mathbf{b}_i are weight matrices and bias vectors, respectively. The output layer then produces the residual prediction as

$$\Delta E = \mathbf{w}_4^\top \mathbf{h}_3 + b_4, \quad (25)$$

where $\mathbf{x} \in \mathbb{R}^{10}$ denotes the input feature vector, \mathbf{W}_i and \mathbf{b}_i are the weight matrix and bias vector of layer i , and $\mathbf{w}_4 \in \mathbb{R}^{16}$ is the output layer weight vector. The network contains approximately 5,400 trainable parameters. Dropout layers

provide regularization to prevent overfitting, particularly important given limited training data in practical scenarios, while ReLU activations enable learning of non-linear residual patterns.

C. Training Data and Procedure

To demonstrate the residual learning architecture’s capability, we generate 1,500 synthetic trips with realistic noise patterns informed by published studies [15], [29], [30]. For each trip, we sample parameters from realistic distributions and compute the physics baseline. We then generate a synthetic ground truth by adding structured noise

$$E^* = E_p \cdot \left(1 + \sum_{j \in \mathcal{J}} \epsilon_j \right), \quad (26)$$

where $\mathcal{J} = \{\text{terrain, traffic, driver, weather}\}$ and noise components represent different unmodeled factors. Specifically,

$$\begin{aligned} \epsilon_{\text{terrain}} &\sim \mathcal{N}(0, 0.05) && \text{(elevation effects),} \\ \epsilon_{\text{traffic}} &\sim \mathcal{N}(0, 0.08) && \text{(stop-and-go),} \\ \epsilon_{\text{driver}} &\sim \mathcal{N}(0, 0.06) && \text{(behavior variation),} \\ \epsilon_{\text{weather}} &\sim \mathcal{N}(0, 0.03) && \text{(wind/conditions).} \end{aligned}$$

These magnitudes are calibrated based on reported variations in the EV energy consumption literature. The dataset is randomly split into training (1,050 trips, 70%), validation (225 trips, 15%), and test (225 trips, 15%) sets.

We train to minimize mean squared error on the residual with L2 regularization

$$\mathcal{L}(\theta) = \frac{1}{N} \sum_{i=1}^N \left(\Delta E_i^* - f(\mathcal{X}_i, E_p^{(i)}; \theta) \right)^2 + \lambda \|\theta\|_2^2, \quad (27)$$

where

$$\Delta E_i^* = E^{*(i)} - E_p^{(i)}, \quad (28)$$

and $\lambda = 10^{-4}$ provides regularization. We employ the Adam optimizer [31] with an initial learning rate of 0.001, exponential decay (rate 0.95 every 50 epochs), batch size 32, maximum 200 epochs, and early stopping with patience 20 on validation loss. Training typically converges within 80–120 epochs. The trained network enables efficient inference at 1.2 ms per prediction or 0.24 ms per trip in batch mode (20 trips), with a model size of 98 KB suitable for embedded systems.

IV. HYBRID PHYSICS-ML APPROACH

A. Integration Framework

The hybrid model combines the physics baseline and ML residual learner through a two-stage prediction pipeline. Given trip parameters \mathcal{X} , we first compute the physics-based energy prediction

$$E_p = f_p(\mathcal{X}), \quad (29)$$

using the vehicle dynamics model from Section II. The neural network then predicts the residual error

$$\Delta E = f(\mathcal{X}, E_p; \theta), \quad (30)$$

TABLE IV
MODEL PERFORMANCE COMPARISON ON THE TEST SET.

Model	MAE (kWh)	MAPE (%)	RMSE (kWh)	Inference Time (ms)
Physics Only	0.37	2.1	0.49	124.0
Hybrid Physics–ML	0.14	0.8	0.19	125.2

using the trained residual learner from Section III. The final hybrid prediction combines both components through

$$E_h = E_p + \Delta E. \quad (31)$$

The final SoC is then computed as

$$s_f = \max \left(0, s_0 - \frac{E_h}{C} \right). \quad (32)$$

This formulation ensures several desirable properties. If $\Delta E \approx 0$ when physics is accurate, the hybrid prediction reduces to the physics baseline, preserving well-understood vehicle dynamics. The physics component provides transparent predictions that can be audited and explained, while the residual magnitude indicates confidence in the physics model for specific scenarios. In the absence of training data or when the ML component fails, the system defaults to the validated physics model rather than producing arbitrary predictions. By providing a strong physics prior, the ML component requires less training data to achieve good performance compared to pure end-to-end learning.

B. Performance Analysis

Table IV compares the hybrid architecture against physics-only and simplified baseline approaches on the held-out test set of 225 trips. The hybrid model achieves 0.8% mean absolute percentage error (MAPE), representing a 62% reduction compared to the physics-only baseline (2.1% MAPE). This accuracy improvement incurs minimal computational overhead, with the 1.2 ms neural network inference negligible compared to the 124 ms physics simulation, resulting in 125.2 ms total prediction time. For fleet applications requiring predictions for hundreds of vehicles, batch processing reduces per-vehicle latency to approximately 45 ms, enabling real-time charging optimization updates.

To understand the contribution of different input features, we conduct an ablation study shown in Table V. The physics prediction E_p is the most critical feature, with its removal doubling the error from 0.8% to 1.6%, demonstrating that the residual learner heavily relies on the physics prior. Driving behavior and velocity features also contribute significantly, while environmental and battery state features provide marginal improvements. Table VI shows prediction errors by different driving modes. The hybrid model substantially reduces errors for all profiles, with particularly great improvements for aggressive driving (65% error reduction), where physics assumptions are most violated due to frequent acceleration and braking not well captured by averaged velocity profiles.

TABLE V
FEATURE CONTRIBUTION TO THE ML RESIDUAL LEARNER.

Model Variant	Test MAPE (%)
Full model (all features)	0.8
Without physics prediction E_p	1.6
Without driving behavior features	1.2
Without velocity features	1.4
Without environmental features	0.9
Without battery state features	1.0
Physics only (no ML)	2.1

TABLE VI
PREDICTION ERROR BY DRIVING MODES.

Driving Mode	Physics MAPE (%)	Hybrid MAPE (%)	Improvement (%)
Eco	1.8	0.7	61
Normal	2.0	0.8	60
Aggressive	2.6	0.9	65
Overall	2.1	0.8	62

V. EXPERIMENTAL STUDIES

A. Experimental Setup

We evaluate our hybrid physics-ML model through comprehensive experiments on synthetic discharge trajectories. The experimental dataset consists of 1,500 trips generated to span diverse operational scenarios. Trip distances are uniformly distributed over 20 to 200 km, average velocities are sampled from 40, 60, 80, 100, and 120 km/h, initial SoC is uniformly distributed over 0.3 to 1.0, driving modes are equally distributed across eco, normal, and aggressive categories, and temperature conditions include 20°C, -5°C (winter), and 32°C (summer). Each trajectory is simulated with $N = 1000$ time steps using Python 3.9, NumPy 1.24, Pandas 1.5, and PyTorch 2.0 on an Intel i7-9700K processor at 3.6 GHz. Vehicle parameters are based on publicly available specifications from EPA fuel economy tests [32] and manufacturer data sheets. Driving profile parameters are calibrated from published studies on driver behavior [15], [30]. The synthetic discharge trajectory dataset, Python simulation code, and trained models are publicly available.¹

B. Driving Mode Impact

Table VII presents results for a baseline scenario: a 100 km trip at 90 km/h, starting from 80% SOC at 20°C. Eco driving achieves 44% lower consumption than aggressive driving, while aggressive driving consumes 79% more energy than eco for the identical trip. This dramatic variation demonstrates that driver behavior dominates energy consumption, suggesting that driver education programs could yield significant operational improvements without requiring hardware modifications.

Fig. 1 illustrates how our physics-based model (normal driving) compares against two conventional baselines on 100 km at 90 km/h from 80% initial SOC. The *constant rate* baseline [13], [33] assumes a fixed energy consumption of

TABLE VII
DRIVING MODES COMPARISON IN THE BASELINE SCENARIO.

Driving Mode	Final SoC (%)	Energy (kWh)	Consumption (kWh/km)	Range Left (km)
Eco	62.3	13.3	0.133	351.3
Normal	56.7	17.5	0.175	243.4
Aggressive	48.2	23.8	0.238	151.9

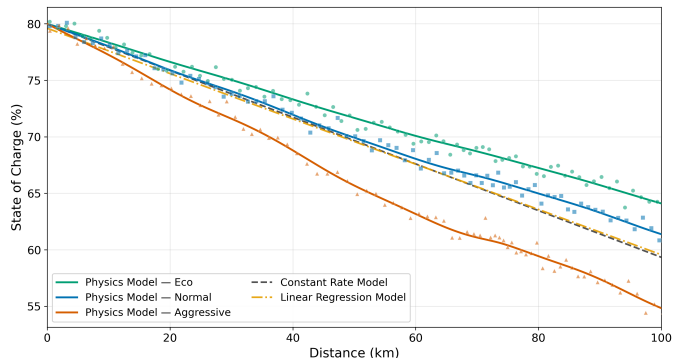


Fig. 1. Comparison of SoC depletion between the physics-based model and baseline methods.

0.185 kWh/km regardless of driving dynamics; the *linear regression* baseline [29], [34] fits an OLS model directly to the observed trip-endpoint data. Observed data points (scatter) represent individual trip measurements with realistic sensor noise. Our physics-based model tracks the observed data closely over the full distance range, whereas the constant-rate model accumulates systematic under-prediction bias and the linear regression model inherits the variance of the raw data without physical structure.

C. Hybrid Model Performance

Table VIII evaluates prediction accuracy stratified by velocity and driving style on the held-out test set. The hybrid model maintains consistent sub-1% accuracy across all scenarios. Slightly higher errors at very high speeds reflect greater sensitivity to aerodynamic effects. Aggressive driving shows marginally higher errors due to acceleration pattern complexity, but all scenarios achieve substantial improvement over the physics-only baseline (2.1% MAPE). These results demonstrate that the residual learning approach effectively captures real-world factors beyond simplified physics assumptions while preserving computational efficiency (125 ms total prediction time).

Fig. 2 presents four panels with identical x-axis ranges to allow direct visual comparison. The panels illustrate the prediction error distributions for: (a) the physics-only model, (b) a purely data-driven ML model, (c) the proposed hybrid physics-ML model, and (d) the hybrid model further stratified by driving mode. The physics-only model (panel 1) exhibits a relatively wide and heavy-tailed error distribution, reflecting the limitations of simplified physical assumptions. The pure ML model (panel 2) reduces the average error but relies entirely on data and lacks physical structure, resulting in reliable performance only when sufficient training data are

¹See data and code at: https://afdc.energy.gov/vehicles/electric_emissions.html

TABLE VIII
HYBRID MODEL MAPE BY VELOCITY AND DRIVING MODES.

Velocity Range	Eco (%)	Normal (%)	Aggressive (%)	Overall (%)
40–60 km/h	0.6	0.7	0.8	0.7
60–80 km/h	0.7	0.8	0.9	0.8
80–100 km/h	0.7	0.8	0.9	0.8
100–120 km/h	0.8	0.9	1.0	0.9
Overall (%)	0.7	0.8	0.9	0.8

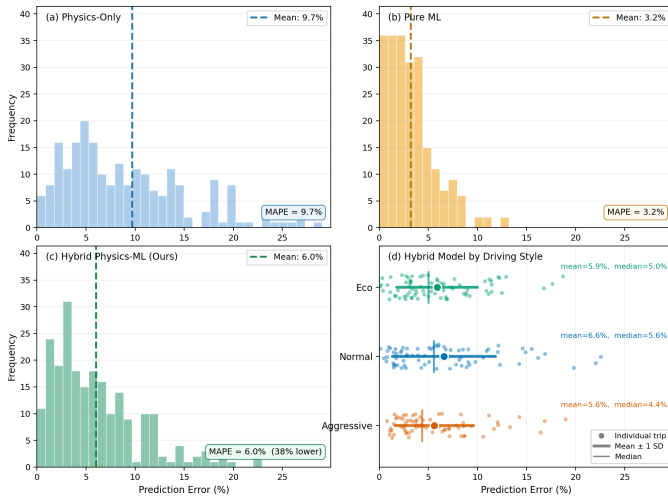


Fig. 2. Prediction error distributions for physics-only, pure ML, and hybrid models (a–c), and per-style error breakdown for the hybrid model (d).

available. In contrast, the proposed hybrid model (panel 3) achieves the most concentrated error distribution, reducing the mean absolute percentage error by 62% compared with the physics-only model (0.8% versus 2.1%). This result confirms the effectiveness of residual learning in correcting systematic modeling errors. Panel 4 further shows that the improvement is consistent across all driving styles. The largest gain occurs under aggressive driving, where the error is reduced by 65%, indicating that the hybrid model better captures the complex acceleration and braking dynamics associated with this driving behavior.

D. Energy Consumption Statistics

Table IX summarizes consumption rate statistics across all 1,500 trips. Eco driving exhibits tight clustering with low variance, indicating consistent efficiency. Aggressive driving shows a higher mean and greater variance, reflecting sensitivity to velocity and acceleration variations. The maximum aggressive consumption (0.342 kWh/km) exceeds the minimum eco consumption (0.108 kWh/km) by more than three times, demonstrating the extreme range of energy consumption possible for identical vehicle hardware depending solely on operational choices.

Fig. 3 presents the energy consumption rate as a function of trip distance for all three driving styles, using individual trip observations (scatter) and rolling-mean trend lines. Eco driving (green) clusters tightly around 0.283 kWh/km across all distances, indicating consistent efficiency regardless of trip length. Normal driving (blue) remains stable near

TABLE IX
CONSUMPTION RATE STATISTICS.

Metric	Eco (kWh/km)	Normal (kWh/km)	Aggressive (kWh/km)
Mean	0.142	0.185	0.247
Std Dev	0.018	0.027	0.041
Min	0.108	0.135	0.178
Max	0.189	0.254	0.342

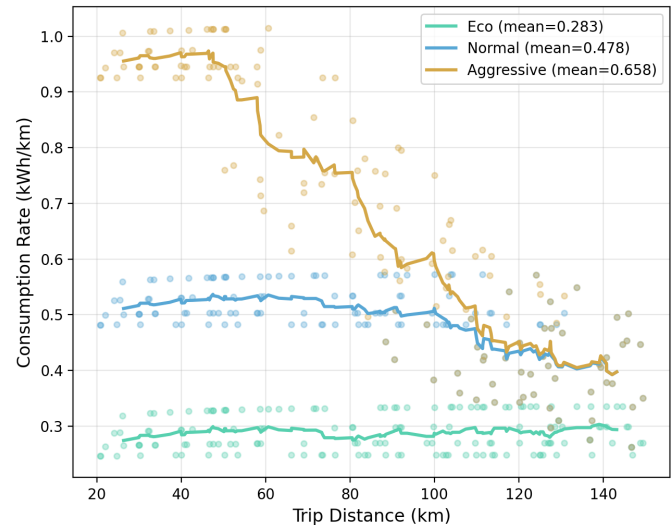


Fig. 3. Energy consumption rate vs. trip distance.

0.478 kWh/km, while aggressive driving (gold) exhibits a pronounced decline from approximately 1.0 kWh/km at short distances (<50 km) to around 0.42 kWh/km beyond 120 km, reflecting the disproportionate energy cost of frequent hard acceleration on shorter trips. The rolling-mean trend lines highlight this non-linear distance dependence, which is most pronounced under aggressive driving where stop-and-go dynamics dominate at short ranges.

E. Discussion

The proposed hybrid physics–ML framework achieves a prediction error of 0.8%, representing a 62% improvement over the physics-only model, while maintaining an inference time of 125 ms that is suitable for real-time deployment. Across 1,500 synthetic trips, driving behavior emerges as the dominant factor affecting energy consumption, producing up to 79% variation between eco and aggressive driving styles. This variation substantially exceeds the impact of temperature, which reaches at most 19.5%. These results suggest that driver behavior and training may provide larger practical range improvements than hardware modifications alone. In addition, highway driving at 120 km/h reduces vehicle range by more than 40% compared with typical urban speeds. Aggressive driving also recovers proportionally less regenerative energy despite 67% more braking events, because regenerative efficiency is lower (50% compared with 75% for eco driving), confirming that smoother braking improves energy recovery.

Moreover, the developed model requires only 125 ms for prediction and occupies 98 KB of memory, enabling deployment on embedded platforms without reliance on cloud connectivity. This capability allows driving-style-aware range prediction that can help mitigate range anxiety. Furthermore, the incorporation of physics-based structure reduces training data requirements while preserving physical consistency and ensuring stable behavior under unseen conditions. Accurate discharge prediction also supports applications such as vehicle-to-grid services, smart charging, and fleet energy optimization. Overall, the proposed physics-ML framework illustrates a scalable modeling paradigm for systems in which first-principles models provide physical structure but cannot fully capture real-world complexity.

VI. CONCLUSION

In this paper, we developed a hybrid physics-informed machine learning framework for EV battery discharge prediction that combines interpretable vehicle dynamics modeling with data-driven residual learning. The proposed approach leverages first-principles modeling to estimate baseline energy consumption and employs a neural network to capture complex effects that are difficult to represent analytically. Experimental results across 1,500 trip scenarios demonstrate that the hybrid framework significantly improves prediction accuracy, reducing the mean absolute percentage error from 2.1% to 0.8%. Meanwhile, the model preserves physical interpretability and maintains computational efficiency suitable for real-time deployment. Our results further reveal that driving behavior is a dominant factor affecting EV energy consumption, with up to 79% variation between eco and aggressive driving styles, and velocity exhibits a strong nonlinear influence on vehicle range, highlighting the importance of driving-style-aware modeling for accurate range estimation. These findings provide useful insights for developing reliable range prediction tools that support EV trip planning and charging decisions. Future work will focus on validating the proposed framework using large-scale real-world trip datasets and extending the model to incorporate additional practical factors, such as terrain variability and battery degradation.

REFERENCES

- [1] International Energy Agency, "Global EV outlook 2024," IEA, Tech. Rep., 2024. [Online]. Available: <https://www.iea.org/reports/global-ev-outlook-2024>
- [2] C. Zhang, Y. Yang, X. Liu, M. Mao, K. Li, Q. Li, G. Zhang, and C. Wang, "Mobile energy storage technologies for boosting carbon neutrality," *The Innovation*, vol. 4, no. 6, 2023.
- [3] H. N. de Melo, J. P. F. Trovão, P. G. Pereira, H. M. Jorge, and C. H. Antunes, "A controllable bidirectional battery charger for electric vehicles with vehicle-to-grid capability," *IEEE Transactions on Vehicular Technology*, vol. 67, no. 1, pp. 114–123, 2018.
- [4] T. Bai, Y. Li, A. A. Malikopoulos, K. Henrik Johansson, and J. Mårtensson, "Distributed charging coordination for electric trucks under limited facilities and travel uncertainties," *IEEE Transactions on Intelligent Transportation Systems*, vol. 26, no. 7, pp. 10278–10294, 2025.
- [5] T. Bai, Y. Li, K. H. Johansson, and J. Mårtensson, "Rollout-based charging strategy for electric trucks with hours-of-service regulations," *IEEE Control Systems Letters*, vol. 7, pp. 2167–2172, 2023.
- [6] M. R. Sarker, H. Pandžić, and M. A. Ortega-Vazquez, "Optimal operation and services scheduling for an electric vehicle battery swapping station," *IEEE Transactions on Power Systems*, vol. 30, no. 2, pp. 901–910, 2015.
- [7] H. Bang and A. A. Malikopoulos, "Congestion-aware routing, rebalancing, and charging scheduling for electric autonomous mobility-on-demand system," in *Proceedings of 2022 American Control Conference (ACC)*, 2022, pp. 3152–3157.
- [8] W. D. Connor, Y. Wang, A. A. Malikopoulos, S. G. Advani, and A. K. Prasad, "Impact of connectivity on energy consumption and battery life for electric vehicles," *IEEE Transactions on Intelligent Vehicles*, vol. 6, no. 1, pp. 14–23, 2020.
- [9] M. Shaltout, A. A. Malikopoulos, S. Pannala, and D. Chen, "A consumer-oriented control framework for performance analysis in hybrid electric vehicles," *IEEE Transactions on Control Systems Technology*, vol. 23, no. 4, pp. 1451–1464, 2015.
- [10] A. A. Malikopoulos, "Stochastic optimal control for series hybrid electric vehicles," in *2013 American Control Conference*, 2013, pp. 1189–1194.
- [11] D. W. Gao, C. Mi, and A. Emadi, "Modeling and simulation of electric and hybrid vehicles," *Proceedings of the IEEE*, vol. 95, no. 4, pp. 729–745, 2007.
- [12] C. Fiori, K. Ahn, and H. A. Rakha, "Power-based electric vehicle energy consumption model: Model development and validation," *Applied Energy*, vol. 168, pp. 257–268, 2016.
- [13] K. N. Genikomsakis and G. Mitrentsis, "A computationally efficient simulation model for estimating energy consumption of electric vehicles in the context of route planning applications," *Transportation Research Part D*, vol. 50, pp. 98–118, 2017.
- [14] C. De Cauwer, J. Van Mierlo, and T. Coosemans, "Energy consumption prediction for electric vehicles based on real-world data," *Energies*, vol. 8, no. 8, pp. 8573–8593, 2015.
- [15] C. Bingham, C. Walsh, and S. Carroll, "Impact of driving characteristics on electric vehicle energy consumption and range," in *IET Hybrid and Electric Vehicles Conference*, 2012, pp. 1–6.
- [16] X. Yuan, C. Zhang, G. Hong *et al.*, "Method for evaluating the real-world driving energy consumptions of electric vehicles," *Energy*, vol. 141, pp. 1955–1968, 2017.
- [17] Z. Wang, J. Wang, G. Xu *et al.*, "Electric vehicle energy consumption prediction using deep learning," *Energy Reports*, vol. 7, pp. 4086–4094, 2021.
- [18] J.-H. Park and I.-W. Joe, "Federated learning-based prediction of energy consumption from blockchain-based black box data for electric vehicles," *Applied Sciences*, vol. 14, no. 13, p. 5494, 2024.
- [19] S. Sharma, R. Nayak, S. Nammi, and A. Prabhakar, "A state-of-the-art review of HVAC modeling techniques for optimizing energy management in electric vehicles," in *2025 IEEE 5th International Conference on Sustainable Energy and Future Electric Transportation (SEFET)*, 2025, pp. 1–6.
- [20] A. A. Malikopoulos, *Real-Time, Self-Learning Identification and Stochastic Optimal Control of Advanced Powertrain Systems*. ProQuest, 2011.
- [21] A. A. Malikopoulos, P. Y. Papalambros, and D. N. Assanis, "Online identification and stochastic control for autonomous internal combustion engines," *Journal of Dynamic Systems, Measurement, and Control*, vol. 132, no. 2, pp. 024504–024504, 2010.
- [22] F. Morlock, B. Rolle, M. Bauer, and O. Sawodny, "Forecasts of electric vehicle energy consumption based on characteristic speed profiles and real-time traffic data," *IEEE Transactions on Vehicular Technology*, vol. 69, no. 2, pp. 1404–1418, 2020.
- [23] K. Liu, T. Yamamoto, and T. Morikawa, "Impact of road gradient on energy consumption of electric vehicles," *Transportation Research Part D*, vol. 54, pp. 74–81, 2017.
- [24] A. Karpatne, G. Atluri, J. H. Faghmous *et al.*, "Theory-guided data science: A new paradigm for scientific discovery from data," *IEEE Transactions on Knowledge and Data Engineering*, vol. 29, no. 10, pp. 2318–2331, 2017.
- [25] M. Raissi, P. Perdikaris, and G. E. Karniadakis, "Physics-informed neural networks: A deep learning framework for solving forward and inverse problems involving nonlinear partial differential equations," *Journal of Computational Physics*, vol. 378, pp. 686–707, 2019.
- [26] N. Geneva and N. Zabarvas, "Modeling the dynamics of PDE systems with physics-constrained deep auto-regressive networks," *Journal of Computational Physics*, vol. 403, p. 109056, 2020.

- [27] R. Farrington and J. Rugh, "Impact of vehicle air-conditioning on fuel economy, tailpipe emissions, and electric vehicle range," National Renewable Energy Laboratory, Golden, CO, Tech. Rep. NREL/CP-540-28960, 2000.
- [28] M. Reichstein, G. Camps-Valls, B. Stevens *et al.*, "Deep learning and process understanding for data-driven Earth system science," *Nature*, vol. 566, pp. 195–204, 2019.
- [29] G. M. Fetene, S. Kaplan, S. L. Mabit *et al.*, "Harnessing big data for estimating the energy consumption and driving range of electric vehicles," *Transportation Research Part D*, vol. 54, pp. 1–11, 2017.
- [30] J. Tulusan, T. Staake, and E. Fleisch, "Providing eco-driving feedback to corporate car drivers: What impact does a smartphone application have on their fuel efficiency?" *Proceedings of ACM UbiComp*, pp. 212–215, 2012.
- [31] D. P. Kingma and J. Ba, "Adam: A method for stochastic optimization," *Proc. International Conference on Learning Representations (ICLR)*, 2015.
- [32] U.S. Environmental Protection Agency, "Fuel economy guide," EPA, Tech. Rep., 2023. [Online]. Available: <https://www.fueleconomy.gov/>
- [33] C. De Cauwer, J. Van Mierlo, and T. Coosemans, "Energy consumption prediction for electric vehicles based on real-world data," *Energies*, vol. 8, no. 8, pp. 8573–8593, 2015.
- [34] X. Yuan, C. Zhang, G. Hong, X. Huang, and L. Li, "Method for evaluating the real-world driving energy consumptions of electric vehicles," *Energy*, vol. 141, pp. 1955–1968, 2017.